ISSN 0351–2657
HOBUD7 28(1) 103 (2004)

MAGNETIC RECONNECTION IN SOLAR FLARES

B. VRŠNAK[1] and M. SKENDER[2]

[1]*Hvar Observatory, Faculty of Geodesy, University of Zagreb, Kačićeva 26, HR–10000 Zagreb, Croatia*
[2]*Ruđer Boškovic Institute, Bijenička 54, HR–10001 Zagreb, Croatia*

UDC 523.985
Conference paper

Abstract. Various aspects of solar flares are considered in the framework of analytic solutions of the complete set of MHD equations describing the $2\frac{1}{2}-$D Petschek's reconnection model. In particular, we compare the theoretical results with characteristics of two-ribbon flares since they provide spatially resolved measurements of various plasma parameters. We emphasize the evolutionary aspect of the process, focusing on the effects of the change of the current sheet length-to-width ratio, longitudinal-to-transversal field ratio, and the ambient value of the plasma-to-magnetic pressure ratio. These parameters determine the conditions for the onset of fast reconnection, the transition to the turbulent reconnection regime, the spatial distribution of the density and temperature, and the efficiency of the particle acceleration.

Key words: solar flares - reconnection

1. Introduction

A solar flare is an abrupt release of the free energy stored in the coronal magnetic fields. During the flare an intricate preflare magnetic configuration restructures into a relaxed postflare loop system. Such a topological change of the magnetic field is possible only by reconnecting the magnetic field lines. Furthermore, the abrupt energy release in flares requires a sufficiently efficient process, much faster than a simple magnetic field annihilation (cf., Priest, 1982).

The concept of fast reconnection was proposed by Petschek (1964). According to the $2\frac{1}{2}-$D option of the model (Petschek and Thorne, 1967), the current sheet is split into two slow-mode standing shocks (SMSs), which are in addition associated with the upstream rotational discontinuities (RDs).

Under the conditions appropriate for solar flares, the reconnection outflow is supermagnetosonic (Forbes, 1986) and a standing fast mode shock (FMS) is formed at the location where the jet encounters an obstacle. In the following the quantities characterizing the inflow region are denoted by the subscript "0", the intermediate region between RD and SMS by "1", the outflow region between SMSs by "2", and the region downstream of FMS by "3".

The coupled system of jump relations for RD and SMS was solved in an approximate form by Soward (1982), and in the complete form by Skender *et al.* (2003). There are four inflow region quantities that determine the reconnection geometry, the energy release rate, and the outflow plasma parameters: *i*) the plasma-to-magnetic pressure ratio $\beta_0 = p_0/p_{m0}$, where $p_m = B^2/2\mu$; *ii*) the ratio of the transversal and the reconnection-plane magnetic field component $B_{z0}/B_{r0} = \tan\Omega_0$; *iii*) the dimensionless reconnection rate expressed by the perpendicular inflow Alfvén Mach number $M_{A0} = v_0/v_{A0}$; *iv*) the direction α of the inflow. Another relevant feature is the overall geometry of the reconnecting system, generally expressed by the sheet length-to-width ratio λ/δ (Furth *et al.*, 1963; Ugai, 1987).

In this paper we describe how the observable quantities depend on these four parameters, considering only the $\alpha = 90°$ case, i.e., the inflow perpendicular to the current sheet (for $\alpha \neq 90°$ see Skender *et al.* 2002, 2003). We focus primarily to the two-ribbon flare process since it is basically a $2\frac{1}{2}-$D problem. Furthermore, flares of this type are usually large, providing spatially resolved measurements of plasma parameters and the related changes of the coronal magnetic field configuration (e.g., Tsuneta, 1996; Uchida *et al.*, 2001).

2. Two-ribbon Flares

The two-ribbon flare occurs as a consequence of the eruption of a sheared magnetic field arcade, which often embeds the cold prominence plasma. After the arcade/prominence system becomes unstable and erupts, a current sheet is created below the flux rope that contains the eruptive prominence (Figure 1). The current sheet forms between the field lines anchored at the opposite sides of the photospheric magnetic inversion line (Lin and Forbes, 2000; Martens and Kuin, 1989), and the flare arises as a result of the fast reconnection in the sheet. The energy is transported to the chromosphere,

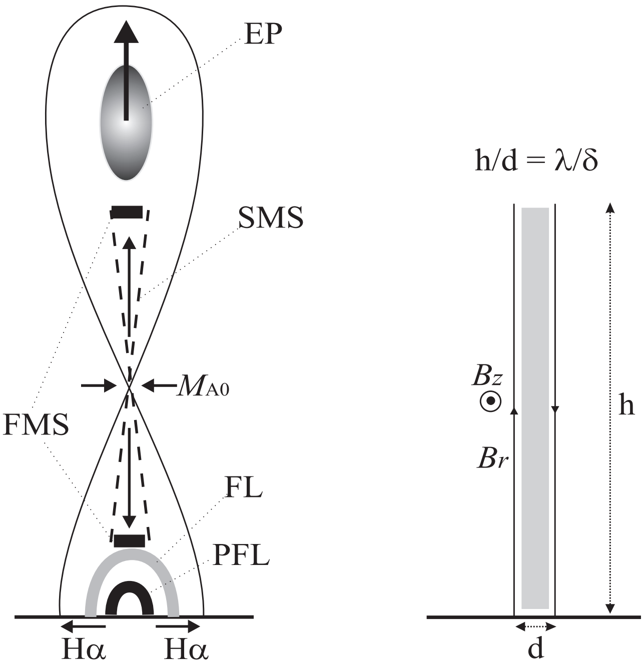

Figure 1: Schematic drawing of two ribbon flare (left): EP – erupting prominence, FL – hot flare loops, PFL – cold postflare loops, Hα – expanding chromospheric ribbons. Right: The current sheet length-to-width ratio.

where two bright ribbons aligned with the inversion line are formed. As the reconnection proceeds, the ribbons expand away from the inversion line and the system of reconnected magnetic loops grows.

In the course of the eruption, the length-to-width ratio of the current sheet increases (Figure 1). At the same time, Ω_0 decreases: since the pre-flare arcade is strongly sheared, there is a significant transversal magnetic field component initially present in the current sheet. As the prominence rises, the overlying arcade field lines are stretched and the inflowing field becomes more and more anti-parallel, i.e., $\Omega_0 \to 0$. Furthermore, the reconnection rate changes: it is initially large, gradually decreasing in the post-impulsive phase of the flare. Finally, as the current sheet rises, weaker fields become involved in the reconnection, i.e., β_0 increases (Gary, 2001). All of these changes are associated with the change of the flare-plasma parameters and the evolution of the energy release modalities.

3. Fast Reconnection Regime

The reconnection can be driven by external flows (Priest and Forbes, 1986), or can be a consequence of the tearing instability (Furth *et al.*, 1963; Ugai, 1987). In the latter case the initiation of the process is usually attributed to a localized (anomalous) resistivity enhancement caused by some of the kinetic plasma instabilities. Such instabilities are easily excited in the current sheet by turbulent flows behind the erupting filament, even before the fast reconnection onset (Vršnak, 1989; Somov, 1992, and references therein).

The fast reconnection regime can set-in only if the length-to-width ratio of the current sheet, λ/δ, is sufficiently large. The analytical treatment of the tearing instability by Furth *et al.* (1963) revealed the critical ratio to be $\lambda/\delta > 2\pi$. Numerical simulations by Ugai (1987) showed a somewhat larger value, $\lambda/\delta > 15$.

In the case of two-ribbon flares this means that the fast energy release cannot start until the eruption attains some critical height: In the course of the eruption the arcade field lines are stretched, and the current sheet elongates. Indeed, Vršnak *et al.* (2003) inferred that in the simple two-ribbon spotless flare of 12 Sept. 2000, the fast reconnection started when $\lambda/\delta > 10$–20. The specifics of this event was that the erupting Hα filament was still visible at the time of flare onset. Measuring the height of the lower edge of the filament, h, and the separation of the flare ribbons, d (Figure 1), it is possible to follow the evolution of the current sheet length-to-width ratio assuming $\lambda/\delta \approx h/d$. It turned out that at the time of the Hα ribbons appearance, the ratio λ/δ was still small, $\lambda/\delta \approx 5$. Yet, in this period the ribbons were static and the soft X-ray flux was only weakly enhanced, indicating that the fast reconnection was still not turned-on. On the other hand, when the ratio attained the value $\lambda/\delta > 10$–20, the ribbons started to expand laterally, revealing the onset of the fast reconnection. At the same time all flare signatures showed a prominent enhancement towards the flare maximum.

After the fast reconnection onset there was a good correlation between the energy release rate and the values of $v_{ch} \times B_{ph}$ measured in the chromosphere, where v_{ch} is the velocity of ribbon expansion and B_{ph} is the photospheric magnetic field (Wang *et al.*, 2003). Bearing in mind the magnetic flux conservation, the quantity $v_{ch} \times B_{ph}$ presumably corresponds to the electric field in the current sheet, $(v \times B)_{cs} \approx v_{ch} \times B_{ph}$ (Vršnak, 1989, Vršnak *et al.*, 1995).

4. Characteristics of the Reconnection Outflow

Let us now consider what happens as Ω_0 decreases, and what is the role of β_0. In Figure 2 we show the current sheet temperature (left) and density (right) as a function of Ω_0. The top panels show the temperature and density jump at SMSs ($T_2/T_1 \equiv T_2/T_0$ and $n_2/n_1 \equiv n_2/n_0$). In the middle panels we show the temperature and density jump at FMS (T_3/T_2 and n_3/n_2). The bottom panels show the temperature (density) downstream of FMS relative to the temperature (density) of the inflowing coronal plasma (T_3/T_0 and n_3/n_0).

The temperature and density excess caused by the reconnection depends primarily on β_0 and Ω_0, whereas the dependence on the reconnection rate is very weak (Skender *et al.* 2003). Bearing in mind that the coronal temperature increases in flares for more than one order of magnitude, one finds that the flares can occur only if $\beta_0 < 0.1$, i.e., β_0 has to be somewhere between 0.1 and 0.01. Similarly, the flare temperatures cannot be reached until Ω_0 decreases below, say, 40°. Note that the hottest plasma, having temperatures almost two times higher than in the rest of the outflow jet, appears behind the FMS which should be located above the post-flare loops. Indeed, super-hot loop-top sources are sometimes resolved in flares (Tsuneta, 1996; Uchida *et al.*, 2001, and references therein).

The dependence of the flare temperature on β_0 is indirectly indicated by some statistical scalings. Ruždjak *et al.* (1989) have shown that on average the temperatures of spotless flares are lower than in spot-group flares. The hottest flares are found to be those in which the Hα emission protrudes over major sunspot umbrae. Moreover, it was demonstrated by Vršnak *et al.* (1991) that in these flares the temperature is proportional to the magnetic field of the involved sunspot. Such a behaviour can be comprehended in terms of the β_0–dependence since stronger field implies a lower β.

At SMS and FMS the plasma is significantly compressed, also having several important observational consequences. Firstly, this has to be taken into account when the heights of radio sources are estimated by assuming that the emission is excited at the local plasma frequency. A straightforward application of some coronal density model would lead to a significant underestimate of the source height – the plasma behind FMS is up to 7

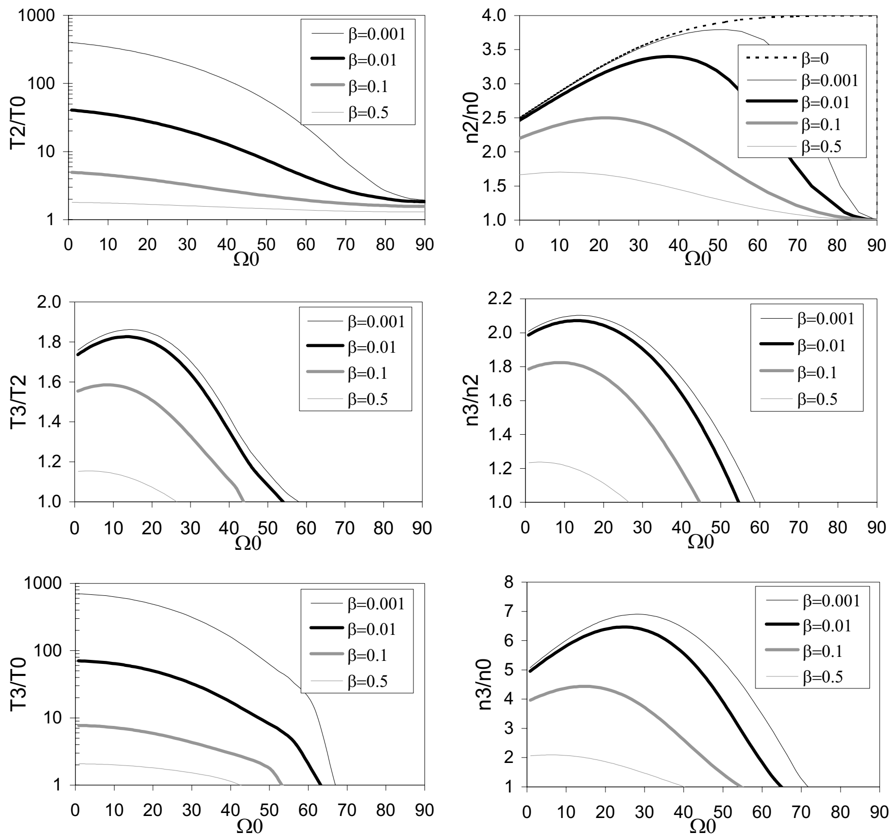

Figure 2: Left: the temperature excess. Right: the density excess.

times denser than in the ambient corona (Figure 2). This can explain how relatively high-frequency sources are found at unexpectedly large heights (Vršnak *et al.*, 2003). The next important aspect is a large density gradient at SMS and FMS. If the plasma radio emission is excited at these discontinuities, the emission is going to be broad-band. For example, a pulsed electron beam passing across SMS would excite a radio pulse of the relative bandwidth $\Delta f/f = \sqrt{n_2/n_0} - 1 \approx 0.6$–$0.9$. Similarly, if the plasma emission is excited at FMS analogously as in the type II bursts, then it should show a band-split of $\Delta f/f \approx= 0.1$–0.2 (Aurass *et al.*, 2002).

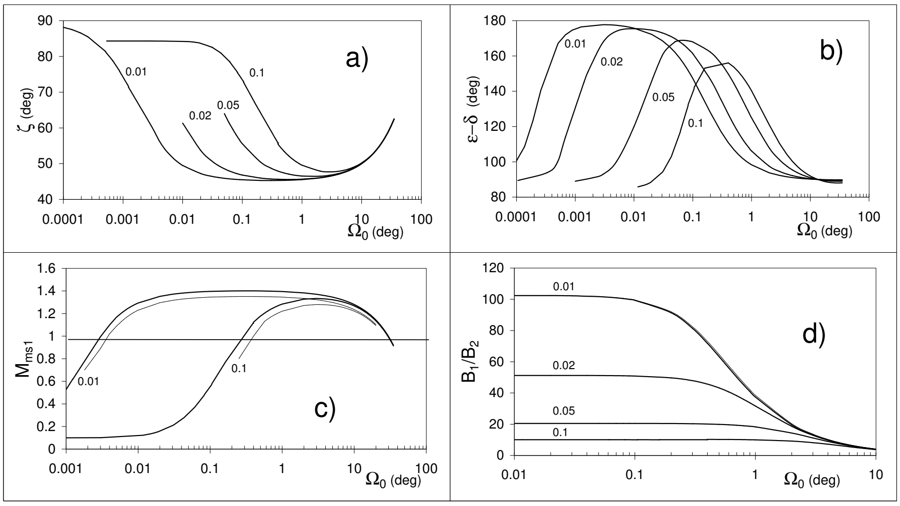

Figure 3: Change of various quantities when $\Omega_0 \to 0$, shown for different reconnection rates M_{A0} (denoted by the curves): a) The angle between the plasma flow and the magnetic field, ζ, in the intermediate region; b) The same for the reconnection-plane components; c) Magnetosonic Mach number M_{ms1} of the flow in the intermediate region d) Magnetic mirror at SMS, B_1/B_2. Full and dashed lines stand for $\beta_0 = 0.01$ and $\beta_0 = 0.1$, respectively.

5. Transition to 2–D Geometry

Skender *et al.* (2003) have shown that in the transition $\Omega_0 \to 0$ the geometry of the system changes dramatically. In Figure 3a we show how the angle between the plasma flow and the magnetic field in the intermediate region, ζ, changes when $\Omega_0 \to 0$. Note the logarithmic scale on the x-axis. The $\zeta(\Omega_0)$ dependence shows a steep increase towards $\zeta \approx 90^\circ$ in the transition to the 2-D case: The change happens within a fraction of a degree.

In Figure 3b we show the change of the angle between the reconnection-plane components of the magnetic field and flow, $\angle(\vec{B}_{r1},\vec{v}_{r1})$, in the intermediate region (δ is the angle between $\vec{B}_{r1}$ and SMS, whereas ε is the angle between $\vec{v}_{r1}$ and SMS; see Skender *et al.*, 2003). Note the sharp peak, $\approx 90^\circ \to 180^\circ \to 90^\circ$, within a fraction of a degree.

In reality however, it is hardly possible that $\Omega_0 = 0$ is strictly satisfied.

Certainly, there are differences larger than $\Delta\Omega_0 = 1^\circ$ present along the current sheet. So, two neighbouring regions of only slightly different Ω_0 are characterized by a large difference in the field/flow direction. This inevitably implies that the MHD turbulence sets-in, meaning that the reconnection has to proceed in a turbulent regime. The current sheet rips in a number of small scale current sheets, which become sites of small-scale reconnections.

Since the growth rate of the tearing instability is proportional to the length scale L of the current sheet ($\tau \approx L/v_A$), the turbulent regime characterized by intermittent formation of numerous small-scale reconnection sheets, can cause a bursty energy release characterized by a sub-second time scale. Furthermore, the reconnection rate in the Petschek regime depends on the length scale as $1/\ln R_m$, where R_m is the magnetic Reynolds number. So, if small scale current sheets are 100 times smaller than the original current sheet, the reconnection rate can be almost five times faster, meaning also that the energy release (per unit volume) can be very powerful locally. Thus, the impulsive phase of two-ribbon flares, generally rich in fine structures, could be a direct consequence of the transition $\Omega_0 \to 0$.

There is another interesting aspect of the transition to the 2-D geometry. In Figure 3c the magnetosonic Mach number M_1 of the flow in the intermediate region is presented as a function of Ω_0. One finds out that in the critical domain, $\Omega_0 \to 0$, there is a regime of supermagnetosonic flows in the intermediate region. Since $M_1 > 1$ is also limited to the very narrow Ω_0 window, one can expect that supermagnetosonic flow creates a shock at the location where it meets a submagnetosonic flow (note that $M_{ms1} > 1$ regime also corresponds to the described change of the field/flow geometry). Inspecting the field/flow directions we infer that supermagnetosonic flows in the intermediate region would create the fast-mode shocks. These shocks could provide pre-acceleration of particles and pre-heating of the plasma inflowing to SMS. This could be essential for generating the high-energy electrons in the current sheet, especially at FMS (Vandas and Karlický, 2000).

The shocks in the intermediate region appear at $\Omega_0 \to 0$, and can be created intermittently all over the current sheet. Thus, they are closely related to the transition towards the turbulent reconnection. Note that M_{ms1} depends on β_0 only weakly, unlike the Mach number of the outflow jet, M_{ms2} (Skender *et al.*, 2003).

6. Particle Trapping and Escape

A very important property of the reconnection system is the large gradient of the magnetic field strength at SMS. So, the plasma in the outflow region is trapped between the two magnetic mirrors at SMSs. The ratio of the magnetic field strengths ($B \equiv B_2/B_1 = B_2/B_0$) depends strongly on the reconnection rate M_{A0} and the shear Ω_0, which is illustrated in Figure 3d. Note that the ratio of B_2/B_1 can be up to 100, and depends only weakly on β_0.

The magnetic mirrors (bottle) are more effective for smaller Ω_0 and slower inflow, and these two quantities are expected to be time-dependent. So, the electron (and proton) distribution functions at different locations change in time, which can influence the flare morphology (see, e.g., Uchida *et al.*, 2001). For example, when the magnetic mirrors become more effective, the energy loss from the current sheet caused by leaking electrons reduces. So, when $\Omega_0 \to 0$, the current sheet temperature rises. Furthermore, a larger number of energized electrons will be approaching FMS, where they are additionally accelerated in a collapsing trap between SMS and FMS (Somov and Kosugi, 1997; Tsuneta and Naito, 1998; Vršnak, 2003) and a larger amount of non-thermal particles can be generated.

Since the outflow Mach number M_{ms2} depends on β_0, it can be expected that the amplitude of FMS decreases in late phases of the flare, after the current sheet shifts to larger heights where β_0 is no more $\beta_0 \ll 1$ (Gary, 2001). This might explain also the revivals of the type IV radio emission – the FMS amplitude presumably enlarges occasionally, when in the inhomogeneous coronal plasma, low β_0 structures once in a while become involved in the reconnection.

Another characteristics of late phases of the flare is that the reconnection rate decreases (presumably due to the increasing length of the current sheet). So, the magnetic bottle becomes more effective, and this can provide a prolonged acceleration of electrons at FMS. This is possibly related also with the hardening of HXR spectrum in time (Brown *et al.*, 1981). Another reason for hardening could be a longer path which electrons have to pass to the chromoshere – the low-energy cut-off of electrons shifts towards the higher energies since the mean-free-path decreases with decreasing electron energy.

7. Conclusion

The presented MHD consideration of the $2\frac{1}{2}-$D reconnection model can explain various aspects of solar flares. Two-ribbon flares provide a comparison between the theoretical expectations and measurements, not only in a qualitative, but also in a quantitative sense. Essential observables are the preflare arcade shear, the current sheet length-to-with ratio, the velocity of ribbon expansion and the corresponding product $v_{ch}B_{ph}$, the temperature of the hot loop-top plasma and its height, etc. However, to get a complete insight into the energy release process, the theoretical aspect should be advanced by including the effects of kinetic plasma processes.

References

Aurass, H., Vršnak, B., and Mann, G.: 2002, *Astron. Astrophys.* **384**, 273.

Brown, J.C., Smith, D.F., and Spicer, D.S.: 1981, in Jordan, S. (ed.), *The Sun as a Star*, NASA SP-**450**, Wshington, p. 181.

Forbes, T.G.: 1986, *Astrophys. J.* **305**, 553.

Furth, H. P., Kileen, J., and Rosenbluth, M. N.: 1963, *Phys. Fluids*, **6**, 459.

Gary, G.A.: 2001, *Solar Phys.* **203**, 71.

Lin., J. and Forbes, T.G.: 2000, *J. Geophys. Res.*, **105**, 2375.

Martens, P.C.H. and Kuin, N.P.M.: 1989, *Solar Phys.* **122**, 263.

Petschek, H.E.: 1964, in Hess, W.N. (ed.), *AAS-NASA Symp on Phys of Solar Flares*, NASA SP-**50**, p. 425.

Petschek, H.E. and Thorne, R.M.: 1967, *Astrophys. J.* **147**, 1157.

Priest, E.R.: 1982, *Solar Magneto-hydrodynamics*, Reidel, Dordrecht.

Priest, E.R. and Forbes, T.G.: 1986, *J. Geophys. Res.* **91**, 5579.

Ruždjak, V., Vršnak, B., Schroll, A., and Brajša, R.: 1989, *Solar Phys.* **123**, 309.

Skender, M., Vršnak, B., and Martinis, M.: 2002, in A. Wilson (ed.), *Solar Variability: From Core to Outer Frontiers*, ESA SP-**506**, 757.

Skender, M., Vršnak, B., and Martinis, M.: 2003, *Phys. Rev. E*, **68**, 0464XX.

Somov, B.V.: 1992, *Physical Processes in Solar Flares*, Kluwer, Dordrecht.

Somov, B.V. and Kosugi, T.: 1997, *Astrophys. J.* **485**, 859.

Soward, A.M.: 1982, *J. Plasma Phys.* **28**, 415.

Tsuneta, S.: 1996, *Astrophys. J.* **456**, 840.

Tsuneta, S., and Naito, T.: 1998, *Astrophys. J.* **495**, L67.

Uchida, Y., Wheatland, M.S., Haga, R., Yoshitake, I., and Melrose, D.: 2001, *Solar Phys.* **202**, 117.

Ugai, M.: 1987, *Geophys. Res. Lett.* **14**, 103.

Vandas, M. and Karlický, M.: 2000, Solar Phys. **197**, 85.

Vršnak, B.: 1989, Solar Phys. **120**, 79.

Vršnak, B.: 2003, in K.-L. Klein (ed.), *Energy conversion and Particle accelerationin the Solar Corona*, *Lecture Notes Phys.*, **612** (Springer, Heidelberg) p. 28

Vršnak, B., Ruždjak, V., Zlobec, P., and Jurač, S.: 1991, Hvar. Obs. Bull., **15**, 1.

Vršnak, B., Ruždjak, V., Altas, L., Ozguc, A., and Zlobec, P.: 1995, Hvar Obs. Bull., **19**, 15.

Vršnak, B., Klein, K.-L., Warmuth, A., Otruba, W., and Skender, M.: 2003, *Solar Phys.*, **214**, 325.

Wang, H., Qiu, J., Ju, J., and Zhang, H.: 2003, *Astrophys. J.* **593**, 564.

MAGNETSKO PRESPAJANJE U SUNČEVIM BLJESKOVIMA

B. VRŠNAK[1] i M. SKENDER[2],

[1] *Hvar Observatory, Faculty of Geodesy, University of Zagreb, Kačićeva 26, HR–10000 Zagreb, Croatia*

[2] *Ruđer Boškovic Institute, Bijenička 54, HR–10001 Zagreb, Croatia*

UDK 523.985

Izlaganje sa znanstvenog skupa

Sažetak. Rješenja potpunog sustava MHD jednadžbi koje opisuju $2\frac{1}{2}-$D Petschekov rekonekcijski model primijenjena su na problem Sunčevih bljeskova. Teorijski rezultati posebice se uspoređuju s dvovlaknastim bljeskovima, kod kojih je moguće vršiti prostorno razlučiva mjerenja različitih plazmenih parametara. Naglašen je razvojni aspekt procesa, pri čemu je posebna pažnja posvećena promjeni omjera duljine i širine strujne plohe, omjera uzdužne i poprečne komponente magnetskog polja, te omjera tlaka plazme i tlaka magnetskog polja. Ovi parametri određuju uvjete za nastup brze rekonekcije i prijelaz u turbulentni režim, te prostornu raspodjelu temperatura i gustoća, kao i efikasnost procesa ubrzanja čestica.

Ključne riječi: Sunčevi bljeskovi - magnetsko prespajanje